JOURNAL OF SOLID STATE CHEMISTRY 111, 164–171 (1994)

Alumina–Metal (Fe, Cr, $Fe_{0.8}Cr_{0.2}$) Nanocomposites

A. Rousset

Laboratoire de Chimie des Matériaux Inorganiques, URA CNRS 1311, Université Paul-Sabatier, 31062 Toulouse Cedex, France

Received November 8, 1993; accepted January 13, 1994

IN HONOR OF C. N. R. RAO ON HIS 60TH BIRTHDAY

Metal (Fe, Cr, $Fe_{0.8}Cr_{0.2}$)/Al_2O_3 composite powders containing from 2 to 20 wt% metallic phase were prepared by selective reduction of oxide solid solutions and studied using mostly TEM and magnetic measurements. The microstructure of the composites is strongly dependent on the morphological and microstructural characteristics of the starting oxide. Most of the metal particles are <10 nm and are dispersed inside the matrix grains. Hydrogen reduction at temperatures <1000°C results in the formation of an iron aluminate spinel phase at the Fe^0/Al_2O_3 interface. Massive composites were prepared by hot-pressing and were found to contain both intragranular (≤30 nm) and intergranular (≤1 μm) metal particles. The former particles are responsible for the strong mechanical reinforcement observed at low metal content, while further enhancement is caused by the latter. Thermogravimetric tests showed that a high metal content and the presence of chromium are beneficial with respect to the resistance to oxidation in air, which is negligible below 1000°C.

INTRODUCTION

The study of systems with a high "surface/volume" ratio such as ultrafine particles or thin films represents a subject in rapid development, although it has been known for a long time that the properties of divided solids are different from those of the same solids in the bulk state (1–3). With the recent progress in preparation and characterization methods, it has now become possible to obtain solid phases whose dimensions are nanometric and which as a result show original physical properties (4). Among these "nanomaterials," nanocomposites consist of materials in which at least one phase is in the nanometer range (5). Ceramic matrix nanocomposites are currently the subject of intensive work (6–8) intended in particular to improve the mechanical properties of ceramics which are known to be brittle. In this field, reinforcement models (9) underline the interest in homogeneous dispersion of submicronic metal particles in a ceramic matrix. In addition, the study of the ceramic/metal interface, as well as that of electrical, magnetic, and optical properties, represents other interesting subjects to consider.

In this paper, we present results obtained on Fe/Al_2O_3, Cr/Al_2O_3, and $Fe_{0.8}Cr_{0.2}/Al_2O_3$ ceramic matrix nanocomposites.

EXPERIMENTAL

The first step in the preparation of the nanocomposite powders consisted of preparing solid solutions of Fe_2O_3, Cr_2O_3, $(Fe_{0.8}Cr_{0.2})_2O_3$, and Al_2O_3 so as to have dispersions of aluminum, chromium, and iron at the atomic level.

Mixed oxalic precursors $(NH_4)_3[Al_{1-x}M_x(C_2O_4)_3]$ (M = Fe, Cr, $Fe_{0.8}Cr_{0.2}$; $0 \le x \le 0.2$) were decomposed in air at 400°C, and the resulting oxide was calcined for 2 hr at different temperatures as required for the study.

The second step corresponded to the reduction in pure, dry hydrogen of the $(Al_{1-x}M_x)_2O_3$ solid solutions to give the M/Al_2O_3 composites. Reduction was carried out at different temperatures and for different times according to the nature of the metallic phase: for iron, 1000°C, 6 hr; for chromium, 1300°C, 5 hr; and for iron-chromium alloy, 1050°C, 20 hr. In addition, a specimen was prepared by reducing an $(Al_{0.9}Fe_{0.1})_2O_3$ solid solution at 600°C for 6 hr.

Massive composites were prepared by hot-pressing the nanocomposite powders at 1450°C under vacuum. The specimens, 20 mm in diameter and 2 mm thick, were ground to 45 μm with a diamond suspension. Relative densities calculated from the mass and dimensions of the specimen were found to be higher than 97%. Thin foils for TEM observations were prepared by mechanical grinding and ionic milling.

The characterization of the powdered and massive composites was mainly carried out by transmission electron microscopy (TEM) and related techniques, X-ray diffraction (XRD), thermogravimetric analysis, magnetic measurements, and Mössbauer spectroscopy.

The fracture strength (σ_f) was measured by the three-point-bending test on parallelepipedic specimens (1.8 ×

0022-4596/94 $6.00

1.8 × 16 mm) machined with a diamond saw. The fracture toughness (K_{IC}) was measured by the SENB method.

RESULTS

1. Nanocomposite Powders

TEM observation of the reduced specimens reveals the formation of a homogeneous dispersion of nanometric metal particles within the grains of the alumina matrix, comparable to that shown in Fig. 1 for a 2 wt% $Fe_{0.8}Cr_{0.2}/Al_2O_3$ composite. Larger metal particles, mostly located in the pores and on the surface of the alumina grains, can also be observed in some specimens (Fig. 2). The microstructure of the metal/ceramic composite powders is indeed closely dependent on several parameters, notably the specific surface area of the solid solution before reduction and its homogeneity.

Irrespective of the transition metal content, an increase in calcination temperature provokes a decrease in the specific surface area, from about 50 m^2/g in the oxides resulting from the decomposition (400°C) to about 2.5 m^2/g in specimens calcined at 1100°C. The influence of the specific surface area of the oxide on the size of the metal particles, as deduced from the measurements of a thousand particles on TEM micrographs, is shown in Fig. 3. In the Fe/Al_2O_3 composites, the average size of the metal particles decreases with a decrease in the specific surface area, whereas it is almost constant (8 nm) in the Cr/Al_2O_3 nanocomposites. This difference in behavior may be due to the lower segregation ratio of chromium in alumina, compared to that of iron (10).

Another parameter to consider is the homogeneity of the oxides before reduction. A recent study (11) has shown that the oxides resulting from the oxalate decomposition were X-ray amorphous and that a single η phase started to crystallize after calcination at a temperature between 750 and 860°C, depending on the composition. The $\eta \rightarrow \alpha$ transition was observed for calcination temperatures higher than 950°C. Analysis of the XRD patterns shows the presence of a α-hematite-rich phase, together with the α-alumina-rich solid solution, in $(Al_{1-x}Fe_x)_2O_3$ specimens with $x > 0.10$, whereas only the latter phase is present for lower iron contents. In agreement with the works of Muan and Somyia (12) showing that chromia enhances the solubility of hematite into alumina, the amount of α-hematite-rich phase is less

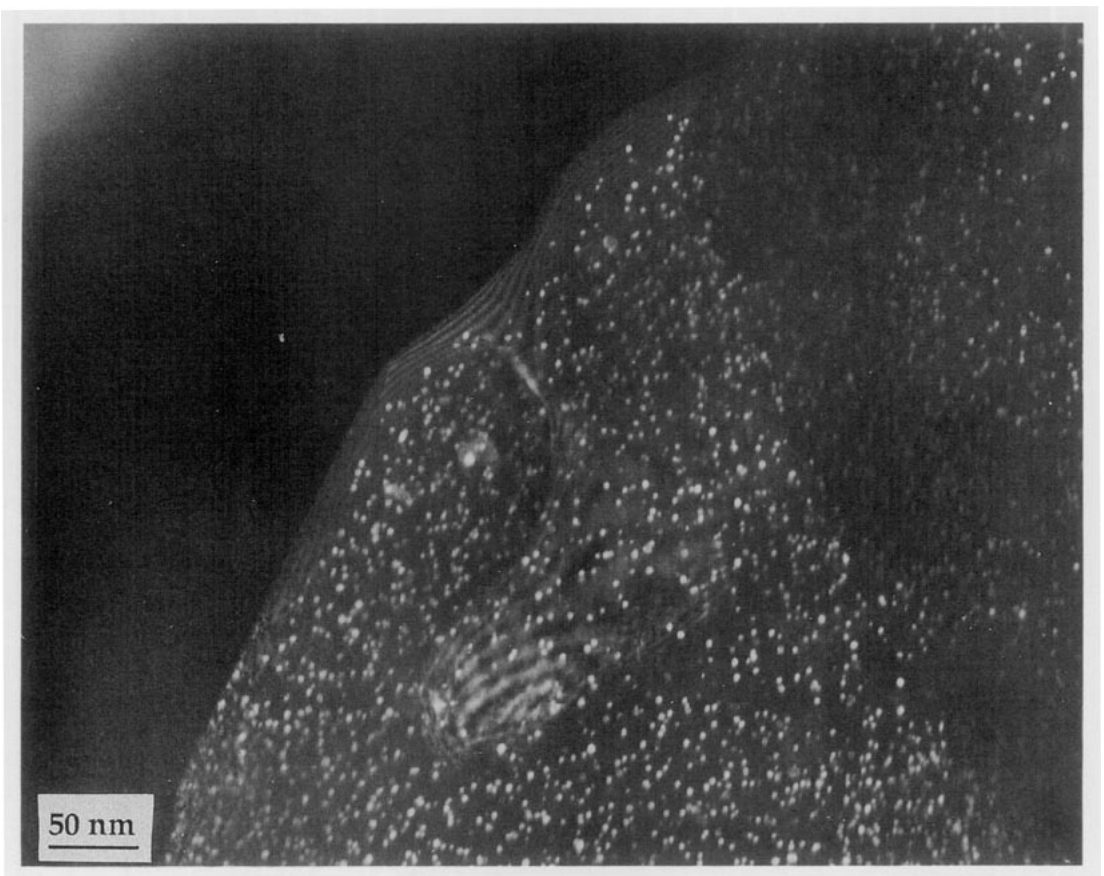

FIG. 1. TEM micrograph (dark field) of a 2 wt% $Fe_{0.8}Cr_{0.2}/Al_2O_3$ composite.

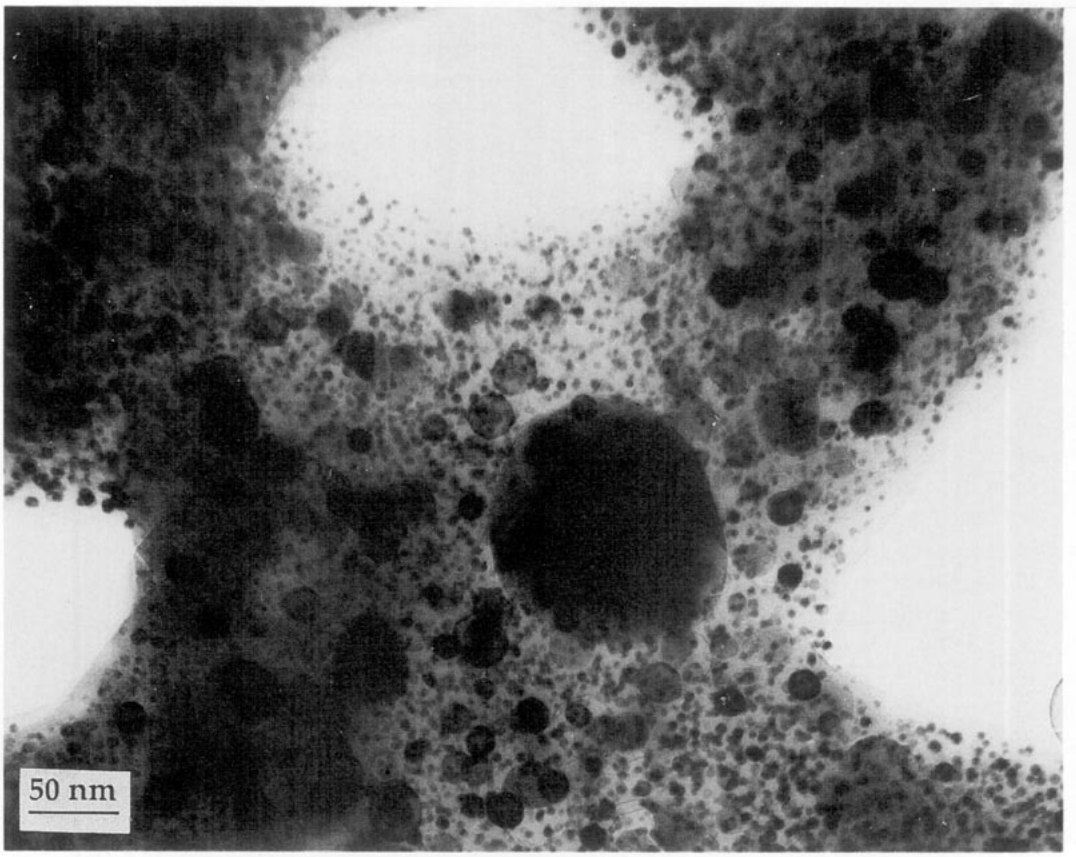

FIG. 2. TEM micrograph of a 20 wt% $Fe_{0.8}Cr_{0.2}/Al_2O_3$ composite.

important in chromium-containing specimens. A single phase is detected in the $(Al_{1-x}Cr_x)_2O_3$ calcined oxides.

If the reduction is carried out on a mixture of phases and not on a single solid solution, the minor, Fe_2O_3-rich phase is easily reduced and gives rise to the formation of metal particles about 30 nm in size, whereas those resulting from the reduction of the Al_2O_3-rich phase are generally smaller than 10 nm. Previous studies (13, 14) have brought to light the high stability of substitutional Fe^{3+} ions in $Al_{2-x}Fe_xO_3$ and shown that the reduction temperatures used in this study were not high enough to totally reduce the Al_2O_3-rich solid solution. However, the addition of metals such as ruthenium and nickel is known to improve the reducibility of the ferric ions (15).

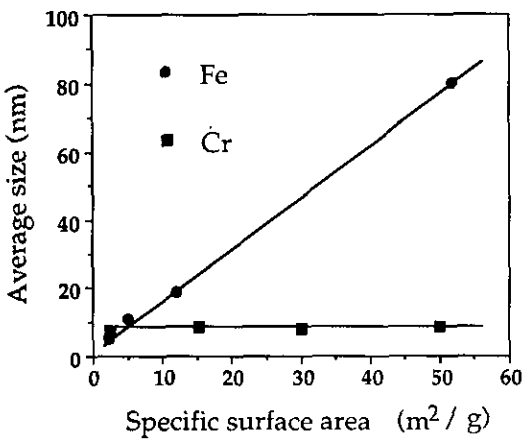

FIG. 3. Average size of the metal particles versus specific surface area of the oxide solid solution before reduction.

Magnetic measurements, in particular the isothermal magnetization curves carried out on the 10 wt% Fe/Al_2O_3 composites between 1.5 and 300 K in fields up to 70 kOe, confirm the relation between the size of the metal particles and the preparation conditions.

We first studied a specimen prepared by reduction at 1000°C of the oxide resulting from the oxalate decomposition; the metal particle size is of the order of 80 nm. The magnetization curves (Fig. 4a) do not vary between 1.5 and 300 K, showing the ferromagnetic behavior of the iron particles.

On the contrary, the magnetization curves obtained with a nanocomposite prepared by reduction at 1000°C of an oxide calcined at 1100°C, in which the average metal particle size is lower than 20 nm, are strongly temperature-dependent (Fig. 4b). At temperatures lower than 10 K the magnetization curves show the superparamagnetic

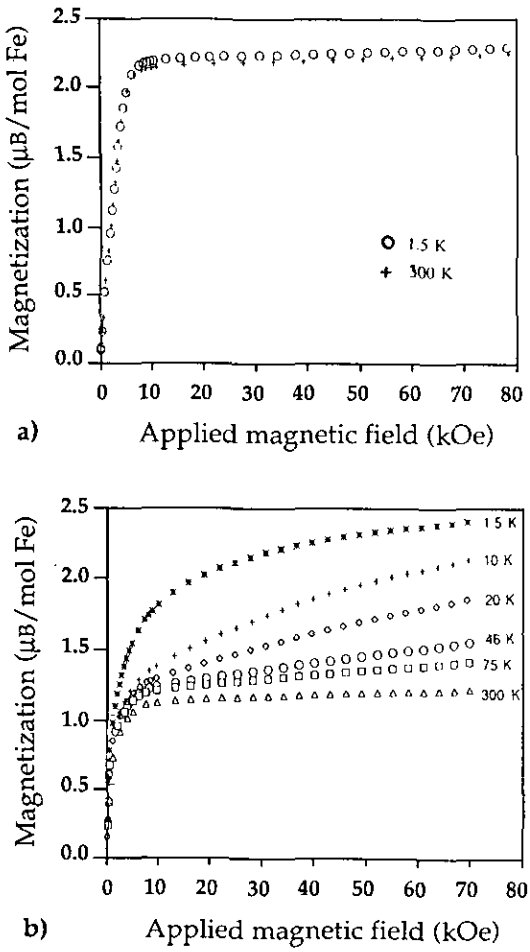

FIG. 4. Isothermal magnetization versus applied magnetic field for 10 wt% Fe/Al_2O_3 composites prepared by reduction at 1000°C of an oxide solid solution of high (a) and low (b) specific surface area.

behavior of the metal particles. It was not possible to obtain saturation in a 70-kOe field at 1.5 K. In addition, saturation magnetization was not obtained at 4.2 K in a 200-kOe field. The shape of the curves shows the existence of at least two different magnetic phases resulting from the bimodal distribution of the iron particles size: on the one hand ferromagnetic particles, several tens of nanometers in size, which are responsible for the spontaneous magnetization at temperatures above 40 K, and on the other hand superparamagnetic iron particles whose size is of the order of a few nanometers. These particles adopt ferromagnetic behavior at low temperature below their blocking temperature, which ranges between a few Kelvin and several tens of Kelvin depending on their diameter.

A high-resolution electron micrograph of this specimen is shown in Fig. 5. The comparison between bright-field and dark-field micrographs, as well as the electron microdiffraction study, show that both the α-alumina grains and the iron particles are monocrystalline and that the intragranular iron particles have the same crystallographic orientation. The indexation of electron microdiffraction patterns leads to the following epitaxial relationship, which was also observed in Cr/Al_2O_3 and $Fe_{0.8}Cr_{0.2}/Al_2O_3$ composites:

$$(111)[\bar{1}\bar{1}2]_M \| (0001)[10\bar{1}0]_{\alpha-Al_2O_3}.$$

However, dislocations are present at the alumina–metal interface to accommodate the lattice mismatch.

A different microstructure is observed in Fe/Al_2O_3 composites prepared by reduction at temperatures lower than 1000°C. In Fig. 6 we show a specimen reduced at 600°C: the iron particles (black) are separated from the alumina matrix (light grey) by an interfacial phase (dark grey).

Magnetic measurements allowed the identification of this phase as an antiferromagnetic iron aluminate ($Fe_{1+x}Al_{2-x}O_4$) with spinel structure: the hysteresis loops obtained at low temperature (<50 K) were found to present a dissymetry; the comparison between the values of the "positive" (H_c^+) and "negative" (H_c^-) coercive fields versus temperature is plotted in Fig. 7. Furthermore, the shift decreases with the number of successive loops at a given temperature. Such a behavior reveals a ferro–antiferromagnetic exchange coupling and the presence of an antiferromagnetic phase at the iron–alumina interface.

2. *Massive Composites*

The massive composites were prepared by hot-pressing the powders elaborated by reduction of oxides calcined at 1100°C so as to minimize the size of the metal particles. The sintering conditions allowed complete reduction of the Fe^{3+} ions which might not have been reduced during the preparation of the powders. The microstructure consists of a bimodal dispersion of metal particles in the α-alumina matrix, the grain size of which is about 2 μm. The metal particles are of different sizes according to their location in the composite (Fig. 8). Those located at the grain boundaries are submicronic, and their size increases from 0.6 to 1 μm with the increase in metal content. Metal particles dispersed inside the alumina grains are generally smaller than 30 nm. TEM and electron microdiffraction studies show that the intragranular metal particles are monocrystalline and are epitaxied in the α-alumina grains according to the same relationship as that found in the powders.

The microstructure of the massive ceramics is directly related to that of the starting powders and to the nature of the dispersed metal. Thus the coalescence of the metal particles is much more important in Fe/Al_2O_3 composites than in $Fe_{0.8}Cr_{0.2}/Al_2O_3$ and Cr/Al_2O_3 specimens.

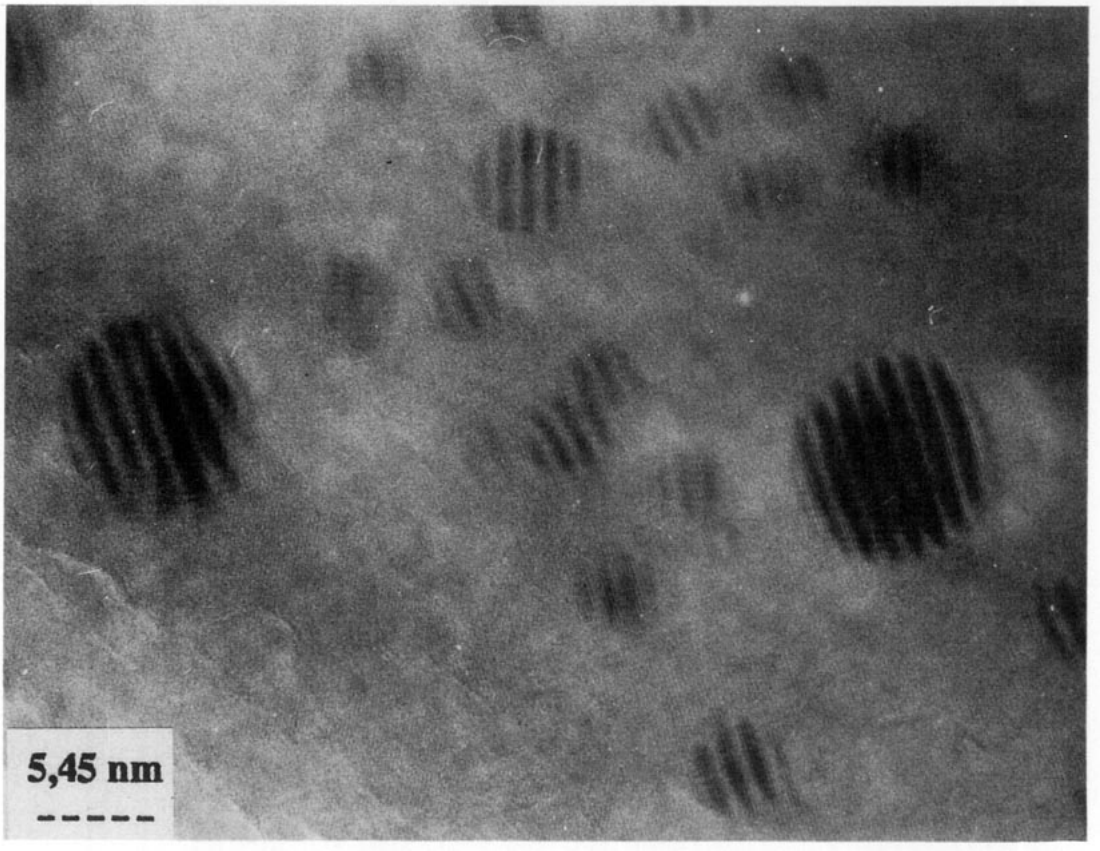

FIG. 5. High-resolution electron micrograph of a 10 wt% Fe/Al_2O_3 composite prepared by reduction at 1000°C.

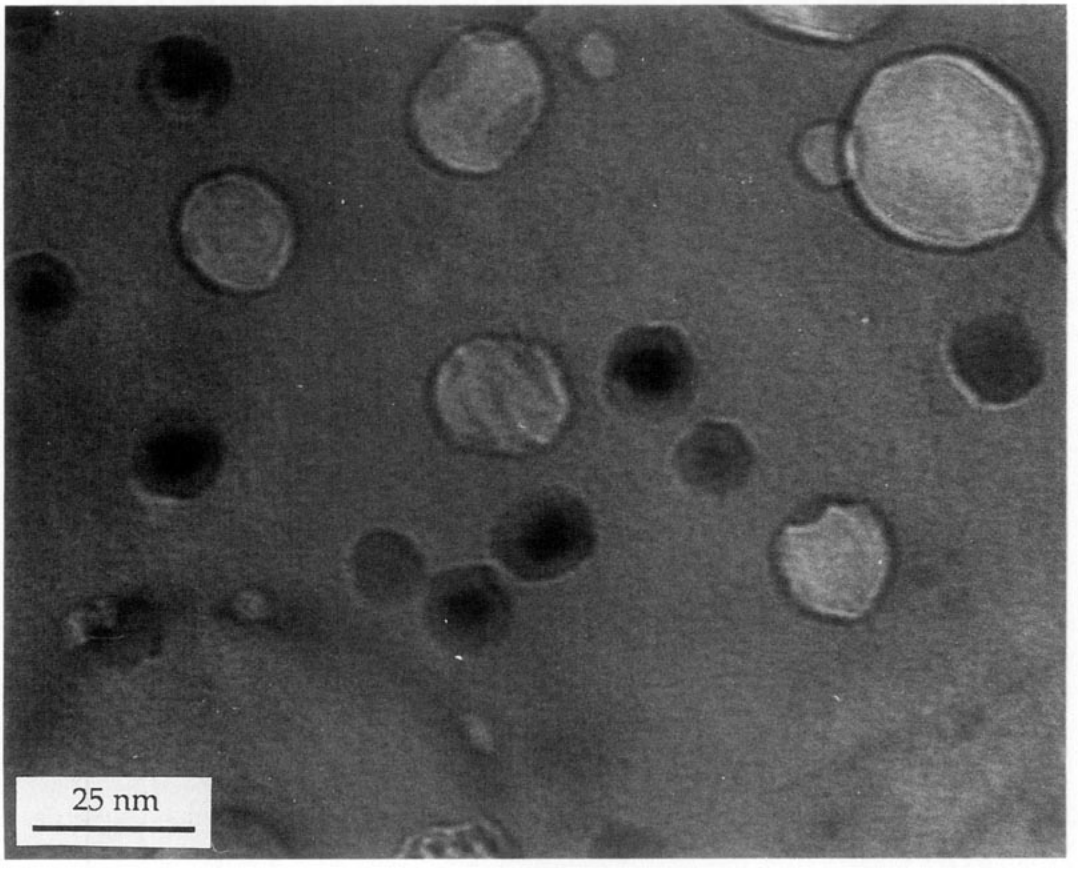

FIG. 6. TEM micrograph of a 10 wt% Fe/Al_2O_3 composite prepared by reduction at 600°C.

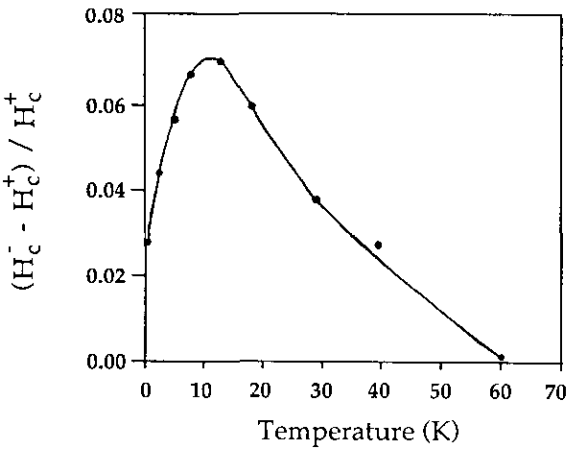

FIG. 7. Shift between the "positive" and "negative" coercive fields for a 10 wt% Fe/Al_2O_3 composite prepared by reduction at 600°C.

The mechanical properties of all the studied composites are higher than those of alumina, the best results being obtained with the 20 wt% $Fe_{0.8}Cr_{0.2}/Al_2O_3$ specimen (Fig. 9). Both the fracture strength and the fracture toughness practically double, reaching values of 860 MPa and 8 MPa$\sqrt{m}$, respectively.

The shape of the curves shows two reinforcement modes. The first one, at low metal contents (<5%), causes a rapid and considerable increase of the mechanical properties. The second one is linked to the presence of submicronic particles dispersed at the grain boundaries of the matrix; its efficiency is greater when the particles are isotropic in shape and their dispersion is homogeneous. Thus our materials may be considered as "micro/nano hybrid composites" (8).

Because of the high sensitivity of metal nanoparticles to oxidation, it was interesting to study their behavior in an alumina matrix. Thermogravimetric analysis experiments were performed on $Fe_{0.8}Cr_{0.2}/Al_2O_3$ massive composite. Test specimens were heated in air up to 1200°C, kept for 1 hr at this temperature, and cooled to room temperature. The proportion of metallic phase that was oxidized during this process, with respect to the total conversion into Fe_2O_3 and Cr_2O_3, is plotted versus metal content in Fig. 10. A surprising result is that the oxidation resistance increases with the amount of metal in the composite. An explanation for this may be found in the microstructure of the composites: specimens containing a low amount of intergranular metal particles are oxidized because oxygen diffusion along the grain boundaries of alumina toward the interior of the material is relatively easy, whereas those containing a high number of metal particles at the grain boundaries are "protected" by the oxidation of these particles, which causes a blocking of

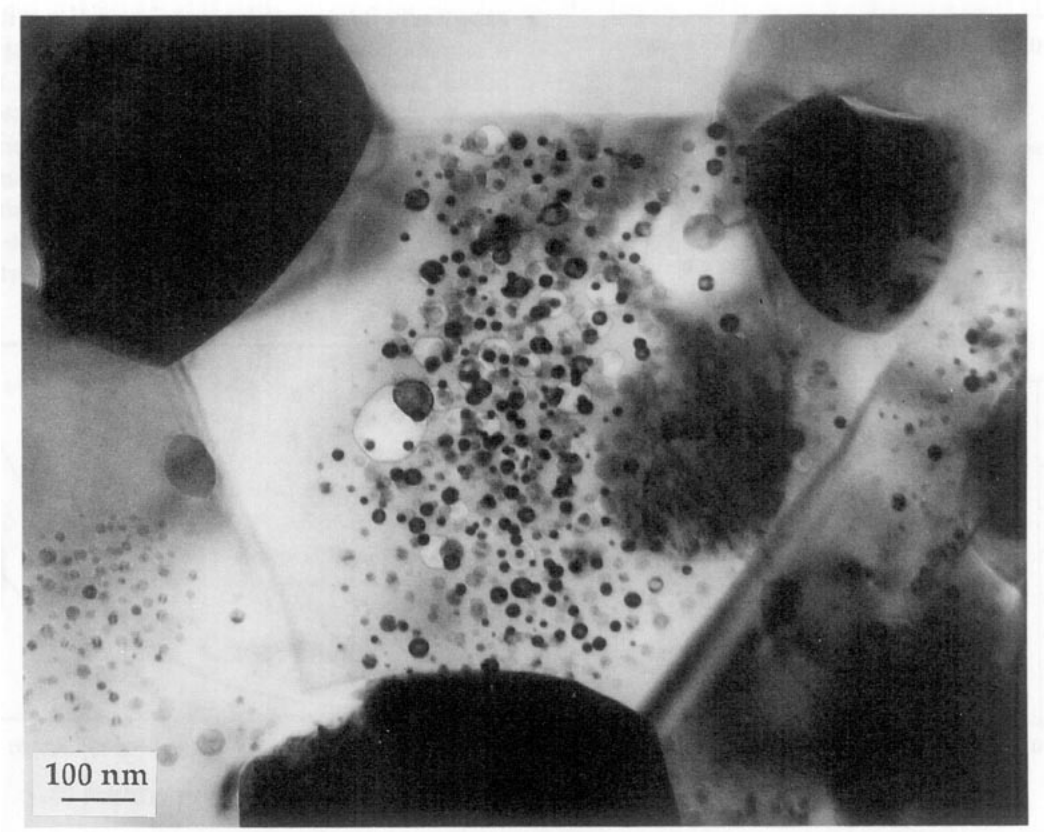

FIG. 8. TEM micrograph of a 20 wt% $Fe_{0.8}Cr_{0.2}/Al_2O_3$ massive composite.

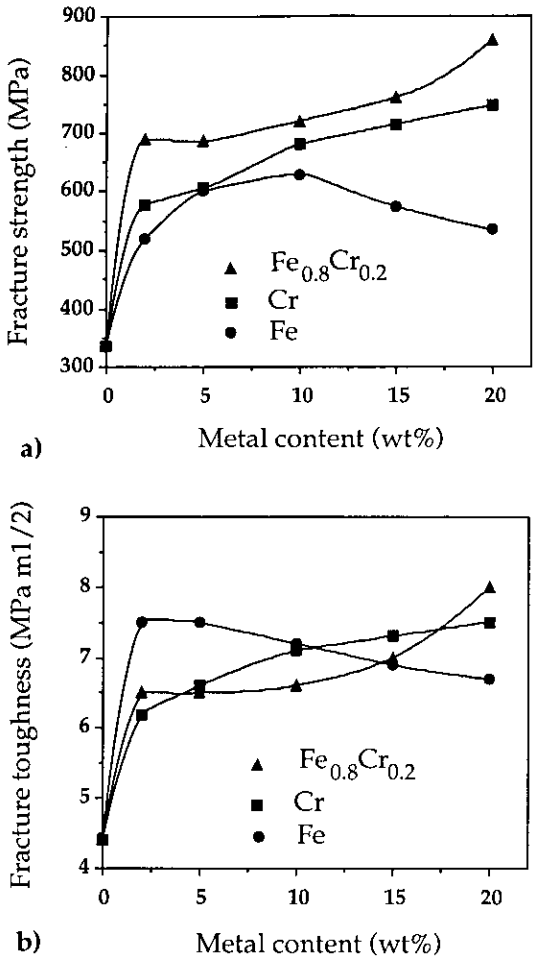

FIG. 9. Fracture strength (a) and fracture toughness (b) versus metal content.

the diffusion path, thus limiting the oxidized fraction of the composite to a surface layer.

Isothermal oxidation tests were also performed on 20 wt% Fe/Al_2O_3 and 20 wt% $Fe_{0.8}Cr_{0.2}/Al_2O_3$ massive composites. Specimens were heated in argon to the desired temperature, at which time air was introduced. The composites were kept for 2 hr at this temperature and cooled to room temperature. Oxidation is negligible below 1000°C, and at higher temperatures is more important for iron particles than for iron–chromium alloy particles (Fig. 11). This protecting effect of chromium is confirmed by a comparison of the Mössbauer spectra before and after oxidation at 1200°C (Fig. 12). The decrease of the relative intensity of the inner sextet, that is clearly detected before oxidation (arrow), shows that the chromium content in the ferromagnetic alloy particles is lower after the thermal treatment.

It is important to note that superparamagnetic metal particles, i.e., nanometric intragranular particles, are still present in the oxidized specimen, as evidenced by the presence of the central singlet in the Mössbauer spectrum (Fig. 12b).

CONCLUSIONS

The elaboration method based on the selective reduction of oxide solid solutions allows the obtainment of essentially intragranular metal particles with a size at the nanometer level. By adjusting the microstructure of the initial powder by means of appropriate thermal treatments, it is possible to control to some extent the size of the metal particles and their intra- or intergranular location, and thus to modify fairly widely the physical and chemical properties of these nanocomposites.

The massive ceramics obtained by hot-pressing have significantly improved mechanical properties compared

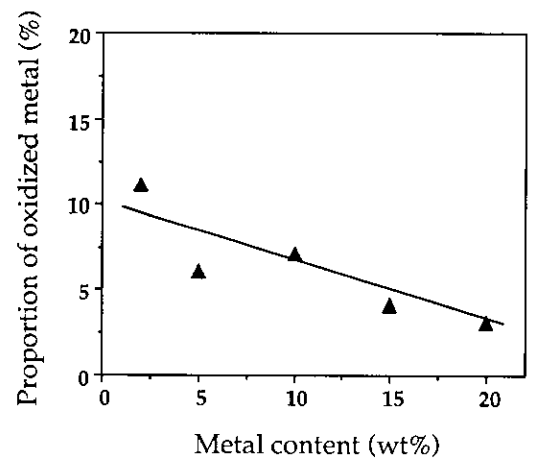

FIG. 10. Proportion of oxidized metal for $Fe_{0.8}Cr_{0.2}/Al_2O_3$ massive composites after heating in air at 1200°C.

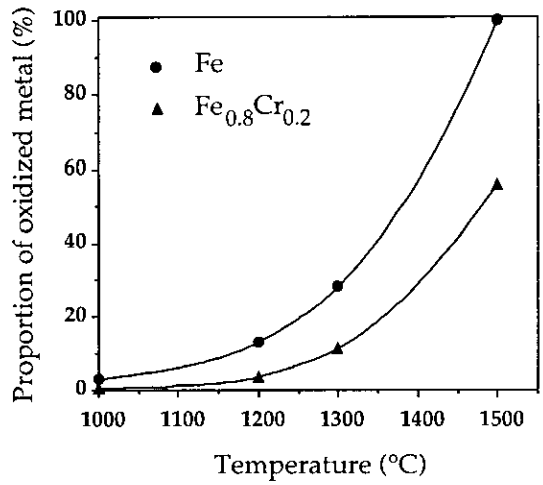

FIG. 11. Proportion of oxidized metal for 20 wt% Fe/Al_2O_3 and 20 wt% $Fe_{0.8}Cr_{0.2}/Al_2O_3$ massive composites.

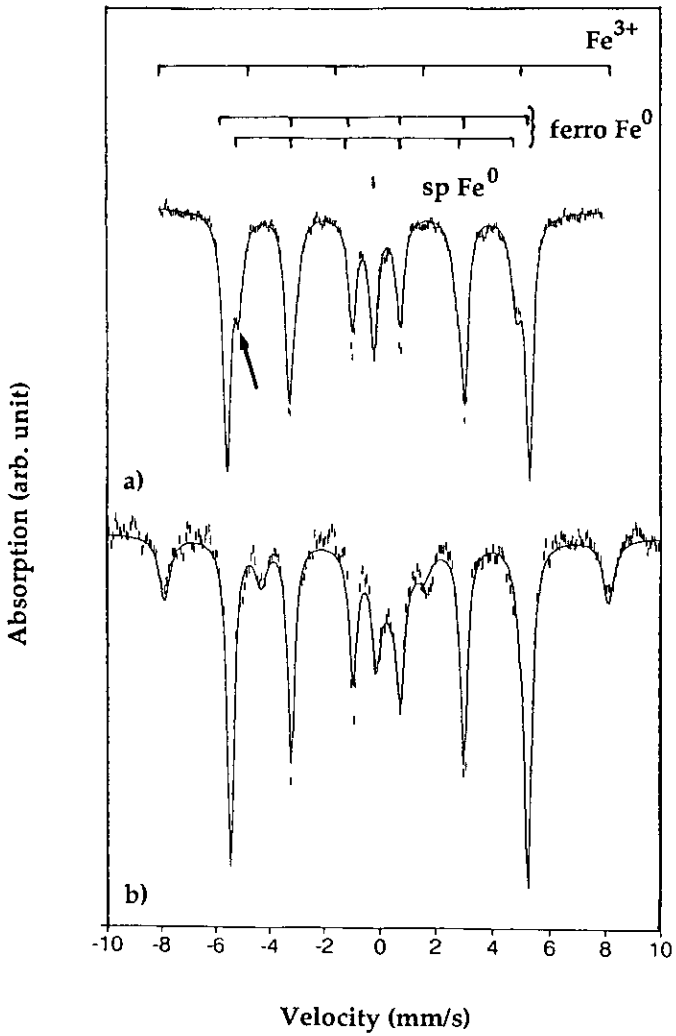

FIG. 12. Room temperature ^{57}Fe Mössbauer spectra of a 20 wt% $Fe_{0.8}Cr_{0.2}/Al_2O_3$ massive composite before (a) and after (b) oxidation at 1200°C. sp, superparamagnetic; ferro, ferromagnetic.

to those of alumina and metal/ceramic microcomposites, as well as a remarkable resistance to oxidation in air up to 1000°C.

The great variety of compositions and microstructures which can be combined in these materials opens up an interesting field of investigation in the structural and functional materials area.

ACKNOWLEDGMENTS

The author thanks B. Barbara, A. Marchand (Laboratoire de Magnétisme Louis-Néel, CNRS, Grenoble, France), X. Devaux, and Ch. Laurent (LCMI, Toulouse, France).

REFERENCES

1. M. Faraday, *Philos. Trans.* **147,** 145 (1857).
2. L. Néel, *Ann. Geophys.* **5,** 99 (1949).
3. P. Mollard, A. Rousset, and J. Paris, "Appareillages et Techniques de Caractérisation des Composés Minéraux Solides," p. 145. Masson, Paris, 1970.
4. H. Gleiter, *Mater. Sci. Eng.* **52,** 91 (1982).
5. R. A. Roy and R. Roy, *Mater. Res. Bull.* **19,** 169 (1984).
6. D. Chakravorty, *Bull. Mater. Sci.* **15,** 411 (1992).
7. S. Komarneni, *J. Mater. Chem.* **2,** 1219 (1992).
8. K. Niihara, A. Nakahira, and T. Sekino, *Mater. Res. Soc. Symp. Proc.* **286,** 405 (1993).
9. A. G. Evans, *Mater. Sci. Eng. A,* **105–106,** 85 (1988).
10. E. Moya and F. Moya, "Non-Stoichiometric Compounds Surfaces, Grain Boundaries and Structural Defects" (J. Nowotny and W. Weppner, Eds.), p. 363. Kluwer Academic, Norwell, MA, 1989.
11. X. Devaux, Ch. Laurent, and A. Rousset, *Nanostruct. Mater.* **2,** 339 (1993).
12. A. Muan and S. Somyia, *J. Am. Ceram. Soc.* **42,** 603 (1959).
13. M. Verelst, K. R. Kannan, G. N. Subbanna, C. N. R. Rao, Ch. Laurent, and A. Rousset, *J. Mater. Res.* **7,** 3072 (1992).
14. Ch. Laurent, A. Rousset, M. Verelst, K. R. Kannan, A. R. Raju, and C. N. R. Rao, *J. Mater. Chem.* **3,** 513 (1993).
15. M. Verelst, K. R. Kannan, G. N. Subbanna, C. N. R. Rao, M. Brieu, and A. Rousset, *Mater. Res. Bull.* **28,** 293 (1993).
16. A. Marchand, X. Devaux, B. Barbara, P. Mollard, M. Brieu, and A. Rousset, *J. Mater. Sci.* **28,** 2217 (1993).